OPTICA

Continuous-wave laser source at the 148 nm nuclear transition of Th-229

Vishal Lal,[1] Maksim V. Okhapkin,[1] Johannes Tiedau,[1] Niels Irwin,[1] Valentin Petrov,[2] and Ekkehard Peik[1,*]

[1]Physikalisch-Technische Bundesanstalt, Bundesallee 100, 38116 Braunschweig, Germany
[2]Max-Born-Institute for Nonlinear Optics and Ultrafast Spectroscopy, Max-Born-Str. 2A, 12489 Berlin, Germany
*ekkehard.peik@ptb.de

Received 24 July 2025; accepted 15 November 2025; published 16 December 2025

A continuous-wave laser source at 148.4 nm based on second-harmonic generation in randomly quasi-phase-matched strontium tetraborate, SrB_4O_7, is demonstrated. It provides $1.3^{+0.7}_{-0.6}$ nW of VUV power in a single pass for an incident UV laser power of 325 mW. The laser system is developed for the resonant laser excitation of the ^{229}Th nucleus to its low-energy isomeric state. For a frequency-stabilized laser system, we expect to reach similar VUV power spectral densities as in previous pulsed laser excitation experiments of the nuclear transition in ^{229}Th-doped crystals.

https://doi.org/10.1364/OPTICA.574489

The recently achieved laser excitation of a low-energy nuclear transition in the isotope Thorium-229 [1–4] has opened a novel domain of nuclear laser spectroscopy. For the first time, to our knowledge, it has become possible to resonantly drive a radiative nuclear transition with a tabletop laser system. Several possible applications have been proposed, including an optical clock with very high accuracy and stability [5,6] and a nuclear γ-ray laser [7]. Methods that have been developed in atomic and molecular laser spectroscopy can now be applied to a nuclear system that offers the advantage of insensitivity to external perturbations predominantly affecting the electron shell. On the other hand, the fact that the nuclear excitation energy of 8.4 eV lies in the same range as excitations of valence electrons may also be used in studies of specific coupling mechanisms between the electron shell and the nucleus, such as an electronic bridge process [8,9]. With a long lifetime $\approx 10^3$ s and a central wavelength of 148.4 nm, exploiting the full potential of the ^{229}Th transition for high-resolution laser Mössbauer spectroscopy or for an optical nuclear clock poses a challenge for the development of ultra-narrow linewidth lasers [10]. In the pioneering experiments with laser sources based on four-wave mixing of ns laser pulses, the obtained linewidths have been limited to the GHz range [1,2], while spectral widths of ^{229}Th lines in the order of 300 [3] and 30 kHz [11] were observed with the seventh harmonic of a fs-laser frequency comb.

The nonlinear frequency conversion efficiency in gases requires high peak intensities, which will either lead to excessive spectral linewidths or, in the case of frequency combs, to rather low power in a single tooth and an ac Stark shift caused by all comb modes [12]. A very promising solution for the generation of narrow-linewidth vacuum ultraviolet (VUV) light is the frequency conversion in acentric optical crystals with second-order nonlinear susceptibility. However, no such crystals have been reported, which are simultaneously transparent at 148 nm and possess sufficient birefringence for phase-matched second-harmonic generation (SHG) at this wavelength. The shortest SHG wavelength of 158.9 nm, recently reported in $NH_4B_4O_6F$ (ABF), still does not permit access to the thorium isomeric state excitation energy of 8.4 eV (148.4 nm) [13]. For sum-frequency generation (SFG), our calculations show that from the available crystals, only $BaMgF_4$ (BMF) is applicable for the target wavelength of 148 nm, but this approach is limited by the very low nonlinear coefficient <0.04 pm/V of the material [14].

When birefringent phase-matching is impossible, quasi-phase matching (QPM) in structured crystals is often the solution to generate the desired wavelength in a three-wave nonlinear process. However, attempts to fabricate QPM structures (e.g., [15–17]) have at present not yielded successful generation of VUV radiation at 148 nm.

In random QPM (RQPM) SHG, waves generated with random phases add up to an SHG power that grows linearly with the crystal length [18]. The shortest wavelength of 121 nm ever reported from a second-order nonlinear optical process was achieved in a RQPM strontium tetraborate SrB_4O_7 (SBO) crystal using a femtosecond laser amplifier [19]. The structure, which originated from a Czochralski growth process [20], contains spontaneously poled domains with opposite orientation normal to the a-axis of the non-ferroelectric SBO. Strontium tetraborate offers a high nonlinear optical coefficient d_{33} (1.5–3.5 pm/V) [19,21], good resistivity to optical damage, and chemical stability. Therefore, RQPM SHG in SBO crystals can be used for a nonlinear optical conversion of continuous-wave (CW) radiation to the vacuum ultraviolet spectral region.

Here, we report the development of an all-solid-state CW laser system for the ^{229}Th nuclear transition, based on three sequential SHG steps starting from a diode laser at 1187 nm. In particular, we demonstrate successful frequency doubling of CW laser radiation

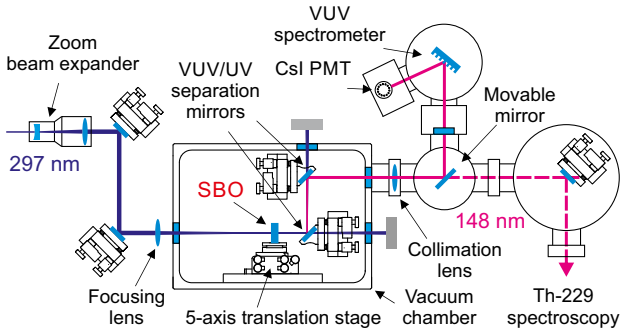

Fig. 1. Experimental setup for SHG at 148.4 nm. UV light at 296.8 nm is focused into the RQPM SBO crystal that generates VUV light. The temperature-stabilized crystal is mounted on a five-axis translation stage. Two dichroic mirrors, a VUV grating, and a solar-blind CsI PMT are used for the detection of the VUV power. The VUV radiation can be directed either to the spectrometer or to the spectroscopy beam line by a mirror mounted on a vacuum-compatible translation stage.

from 296.8 to 148.4 nm in an RQPM SBO crystal previously studied in [19].

The setup for detecting VUV radiation from SHG is designed to be sensitive to very low light powers on the fW level. The SHG process is driven by a commercial frequency quadrupled CW laser (Toptica TA-FHG pro) with an output power of ≈400 mW at a wavelength of 296.8 nm and a specified linewidth in the order of 100 kHz. In this work, we are using the laser without active frequency stabilization.

For SHG, we use the same uncoated SBO crystal with irregular domain structure described in Ref. [19]. The laser radiation is focused into the SBO sample with dimensions of $0.9 \times 6.4 \times 5.6\,\mathrm{mm}^3$ ($a \times b \times c$ crystal axis, respectively, adopting the $Pmn2_1$ space group notations), placed in a vacuum chamber for the final conversion to 148.4 nm (see Fig. 1). The domains have a random thickness from <0.1 to >100 μm along the light propagation direction (crystal a-axis) and a coherence length ∼0.3 μm at this wavelength. The polarization of the incident laser radiation is oriented parallel to the crystal c (z)-axis. The crystal holder provides a rotation of the SBO around the c- and b-axes. It is mounted on a five-axis vacuum-compatible translation stage for fine optimization of the crystal position and orientation. The SBO crystal is temperature stabilized via a Peltier thermoelectric module. At 296.8 nm, we observe transmission losses in this sample on the order of a few percent in addition to the reflection losses of ≈8%. The losses can partially be attributed to minor surface damage from earlier experiments with this crystal under high-intensity UV irradiation. An orientation of the SBO crystal at the Brewster angle is not optimal for SHG due to the increase in period thickness of the complex domain structure.

To find an optimal beam waist in the SBO crystal, we vary the laser beam diameter with a zoom beam expander and focus the beam into the crystal with a 200 mm lens. The total power losses of the optical elements used to direct the UV beam to the SBO sample are ≈20%. Two dichroic mirrors are used for the separation of the VUV and UV beams and to direct the VUV radiation to a detector. The SHG vacuum chamber is separated from the other parts of the vacuum system by a MgF_2 viewport with a transmission of ≈90% at 150 nm. For the collimation of the VUV radiation, we are using a positive MgF_2 lens. Finally, the light is directed into a VUV-spectrometer (HP Spectroscopy easyLIGHT) equipped with a CsI photomultiplier tube (PMT) (Hamamatsu R8487) for the detection of the VUV radiation. The spectrometer is separated from the spectroscopy beam line by a second MgF_2 viewport with the same transmission.

The main challenge for the SHG detection is obtaining sufficient suppression of the fundamental radiation. This requirement can be estimated from the ratio of initial UV power (≈0.3 W) compared to a weak VUV signal in the fW range (under non-optimized conditions), which corresponds to a suppression factor of 14 orders of magnitude. In addition to a solar-blind CsI PMT [22] with a low efficiency in the UV, we use two dichroic VUV/UV separation mirrors in combination with a spectrometer grating for the extraction of the VUV signal from the UV background. The dichroic mirrors are characterized in the UV with a calibrated photon flux, resulting in an estimated attenuation factor of about 100. The combined reflection of the two mirrors in the UV is measured to be $9 \cdot 10^{-5}$. The residual UV reflection from the grating reaches a few times 10^{-5} when the diffraction angle is tuned for 148 nm detection. Finally, a solar-blind PMT detection efficiency of about $5 \cdot 10^{-6}$ is measured with a calibrated light flux at 297 nm. This corresponds to the total attenuation of $\geq 10^{14}$, which is enough to suppress the UV background to the order of 10^3 counts per second.

The overall VUV detection efficiency is calculated from the reflection coefficients of 83% for p-polarization of the mirrors, a diffraction grating efficiency of 0.42 at 148 nm, and a PMT quantum efficiency of 22% ($40.5 \cdot 10^3$ A/W anode radiant sensitivity) given by the suppliers. The previously used MgF_2 optical viewports and the collimation lens [23] have a transmission close to 90% per element. The optical losses are mostly due to Fresnel reflection from uncoated surfaces. The overall VUV detection efficiency, including the uncertainties of all the individual elements, is 4(1)%.

The SHG power is derived from the PMT signal measured using two different detection methods. We detect the signal by counting the VUV photons using a gated photon counter (counting rate up to 200 MHz) and by PMT current measurements. The PMT signal discriminator for the gated counter is chosen in the dark count plateau to avoid an overestimation of the VUV power. However, when the photon counting rate exceeds 10 MHz, we observe a saturation of the count rate determined by the pulse-pair resolution of the PMT. To overcome this effect for the high photon flux, we measure the PMT current of the VUV signal by a picoammeter and take into account the anode radiant sensitivity, as calibrated by the supplier for the specific PMT. We are using two different picoammeter models and observe the same values with an uncertainty of <2%.

The initial alignment of the spectrometer is performed with the fundamental radiation directed to the spectrometer by motorized VUV/UV separation mirrors. After optimizing the UV signal on the PMT, the entire spectrum, including the SHG signal, can be recorded, as shown in Fig. 2. To discriminate against the scattering background and the occurrence of higher-order reflection of the fundamental radiation at the 148.4 nm diffraction angle, a comparison measurement is also performed while the spectrometer is filled with air at atmospheric pressure. As expected, the peak at 148.4 nm disappears due to the absorption of the VUV radiation in oxygen.

The irregular domain structure of the SBO crystal is inhomogeneous across the sample. Therefore, we scan the crystal position relative to the laser beam to find the most efficient points. We found one area with the highest VUV output power and three areas with slightly lower VUV power. The output power observed

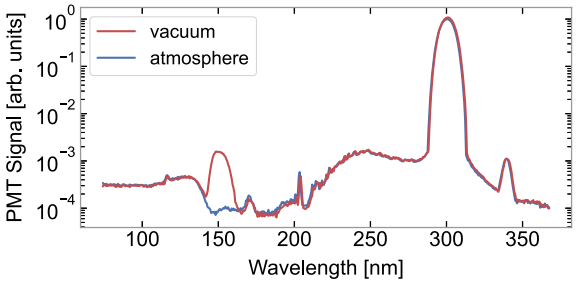

Fig. 2. Recorded PMT signal showing fundamental and second-harmonic spectra. The SHG signal at 148 nm vanishes under atmospheric conditions due to high absorption of the VUV light. The peaks between 170 and 340 nm are residuals of the UV radiation.

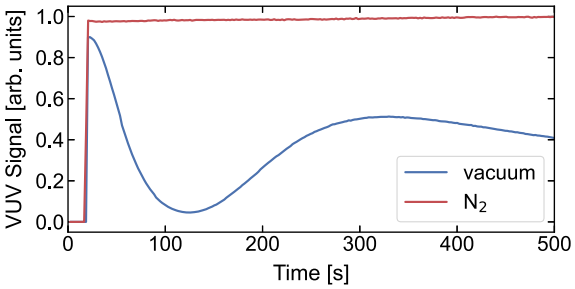

Fig. 3. VUV signal measured with the SBO crystal in vacuum and under high-purity N_2 buffer gas. The laser radiation was initially blocked and then applied to the crystal. The crystal in vacuum shows strong local temperature variations that change the RQPM conditions and therefore the resulting VUV signal.

over the rest of the SBO is significantly lower (10–100 times). Each point requires fine adjustment of the incident UV beam to the crystal position to maximize the output SHG power. We also observe an angular dependence of the SHG power. Small rotations (changes of the effective nonlinear coefficient can be neglected) of the crystal around the *b*- or *c*-axes result in similar changes in the effective domain thickness and therefore SHG power. In our setup, a rotation around the crystal *b*-axis is provided over a wider range. We have found that the optimal incidence angle is ≈9° in the *a*, *c*-plane at room temperature. We assume this orientation better fits the RQPM conditions of the SBO crystal for the wavelength of 148.4 nm. A similar behavior has been described before (e.g., [24]).

For the determination of the optimal beam focusing, the output SHG power is measured as a function of the UV beam waist. We use an additional collimation lens placed after the crystal to avoid the influence of varying beam divergence on the detection. For the SBO sample used in this experiment, we have found that the optimal UV beam waist radius in the crystal lies in the range of 20–25 µm.

As mentioned above, the present SBO crystal exhibits some residual absorption at the fundamental wavelength. The local heating of the sample in a vacuum causes thermal variations of the SHG power. We observe a fast reduction of the VUV power at high UV powers while keeping the setpoint of the temperature stabilization fixed. Filling the chamber with 10^5 Pa of 99.999% purity N_2 gas after pumping to 10^{-4} Pa, the output VUV power remains approximately constant over time (see Fig. 3). We assume that the buffer gas efficiently conducts heat away from the crystal surface and reduces the temperature gradients. This prevents changing the RQPM conditions and the variation of the VUV power. The temperature dependence of the SHG power for different incident laser powers in vacuum and nitrogen buffer gas conditions is shown in Fig. 4. Corrections of the crystal temperature are required for the compensation of the VUV power reduction in vacuum [see Fig. 4(a)]. At a further increased laser power of 250 mW, the optimal SBO operation temperature has to be reduced by ≈10 K relative to the initial RQPM temperature at a laser power of ≤ 50 mW. In nitrogen buffer gas, this temperature correction is not required, and the optimum operation temperature remains constant for a wide range of incident UV powers [see Fig. 4(b)].

The resulting SHG power in dependence on the fundamental incident power is shown in Fig. 5. The process shows a quadratic behavior in the PMT current measurements and the counting mode for UV powers below 225 mW, as expected for the SHG process. Only for the counting method at high UV powers and a detected photon counting rate ≥ 10^7 s^{-1}, we observe a saturation

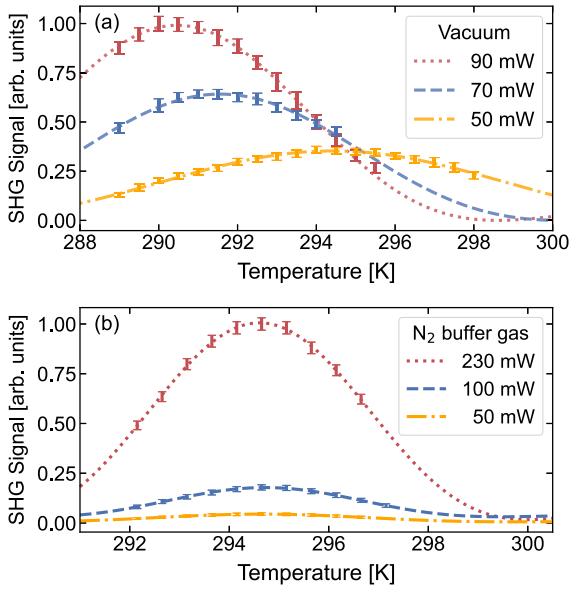

Fig. 4. SHG power as a function of crystal temperature for varying fundamental power under vacuum (a) and N_2 buffer gas environment (b). The dashed lines are fits with sinc^2-functions. In the absence of nitrogen, the optimal temperature for SHG decreases with increased fundamental power due to heating caused by absorption in the crystal.

of the detected counts, as shown in Fig. 5(a). Therefore, the output power measured with photon counting is corrected for this effect. The measured output power is recalculated from the PMT signal using the detection efficiency. The uncertainties shown in Fig. 5(a) include both statistical and systematic contributions. The largest systematic contribution arises from the discrepancy between the two independent methods of measuring power and the uncertainty of the diffraction grating reflectivity [see Fig. 5(b)]. Scanning the laser frequency over ≈10 GHz does not change the SHG power significantly, in agreement with previous calculations presented in [24].

In conclusion, a CW VUV laser source with the VUV power of $1.3^{+0.7}_{-0.6}$ nW at the excitation wavelength of 148.4 nm of the nuclear transition of ^{229}Th has been demonstrated. Using an RQPM SBO crystal, we achieve a significantly shorter CW wavelength in comparison with the previously reported value of 191 nm generated by phase-matched SHG in $KBe_2BO_3F_2$ (KBBF) [25]. The VUV power, which is directed to a spectroscopy experiment (with Th-doped crystals or ions) is reduced by losses at a MgF_2 viewport and

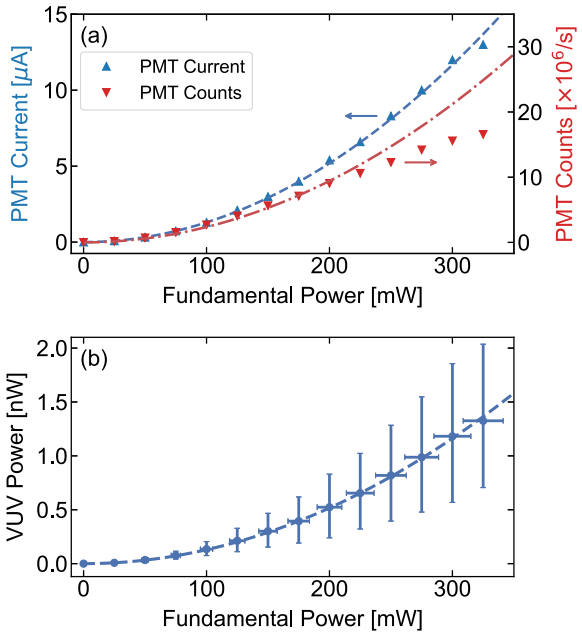

Fig. 5. (a) Typical dependence of PMT VUV current and counts on the fundamental power with quadratic fits. For the photon counting dependence, the fit ignores experimental points at UV powers ≥ 225 mW, where a saturation effect of the photon counting method is observed. (b) SHG power as a function of the fundamental power.

three mirrors. Assuming a minimal VUV power after the crystal of ≈0.7 nW and taking into account all optical losses, we expect to apply ≥ 0.3 nW for investigations of the Th nuclear transition.

The first laser excitation of the isomeric state in a ^{229}Th-doped CaF_2 crystal was achieved using a VUV laser source based on four-wave frequency mixing in xenon [1,23] with the VUV power spectral density of ≈0.1 pW/Hz. With a CW VUV power of 0.3 nW, a linewidth in the kHz range would be required to reach a similar optical power density. For narrow linewidth high-precision spectroscopy, a frequency stabilization system is now under development as employed in various optical clocks (see review [26]). The main limitation of the present VUV laser source based on RQPM in strontium tetraborate is the unique domain structure of individual crystals and, therefore, the unique characteristics of the RQPM conversion efficiency. The problem may be eventually resolved by manufacturing patterned SrB_4O_7 crystals [27].

Funding. European Research Council (856415); Deutsche Forschungsgemeinschaft (274200144); European Union (23IEM03 HIOC).

Acknowledgment. We would like to thank Thomas Leder, Martin Menzel, and Andreas Hoppmann for their technical support.

Disclosures. The authors declare no conflicts of interest.

Data availability. Data underlying the results presented in this paper are not publicly available at this time but may be obtained from the authors upon reasonable request.

REFERENCES

1. J. Tiedau, M. V. Okhapkin, K. Zhang, *et al.*, Phys. Rev. Lett. **132**, 182501 (2024).
2. R. Elwell, C. Schneider, J. Jeet, *et al.*, Phys. Rev. Lett. **133**, 013201 (2024).
3. C. Zhang, T. Ooi, J. S. Higgins, *et al.*, Nature **633**, 63 (2024).
4. C. Zhang, L. von der Wense, J. F. Doyle, *et al.*, Nature **636**, 603 (2024).
5. E. Peik and C. Tamm, Europhys. Lett. **61**, 181 (2003).
6. C. J. Campbell, A. G. Radnaev, A. Kuzmich, *et al.*, Phys. Rev. Lett. **108**, 120802 (2012).
7. E. V. Tkalya, Phys. Rev. Lett. **106**, 162501 (2011).
8. E. V. Tkalya, V. O. Varlamov, V. V. Lomonosov, *et al.*, Phys. Scripta **53**, 296 (1996).
9. S. Matinyan, Phys. Rep. **298**, 199 (1998).
10. K. Beeks, T. Sikorsky, T. Schumm, *et al.*, Nat. Rev. Phys. **3**, 238 (2021).
11. T. Ooi, J. F. Doyle, C. Zhang, *et al.*, arXiv (2025).
12. T. Udem and F. Riehle, La Rivista del Nuovo Cimento **30**, 563 (2007).
13. F. Zhang, Z. Chen, C. Cui, *et al.*, arXiv (2025).
14. E. G. Villora, K. Shimamura, K. Sumiya, *et al.*, Opt. Express **17**, 12362 (2009).
15. M. Shao, F. Liang, H. Yu, *et al.*, Light. Sci. Appl. **11**, 31 (2022).
16. S. Buchter, T. Fan, V. Liberman, *et al.*, Opt. Lett. **26**, 1693 (2001).
17. S. J. Herr, H. Tanaka, I. Breunig, *et al.*, Opt. Mater. Express **13**, 2158 (2023).
18. M. Baudrier-Raybaut, R. Haidar, P. Kupecek, *et al.*, Nature **432**, 374 (2004).
19. P. Trabs, F. Noack, A. S. Aleksandrovsky, *et al.*, Opt. Lett. **41**, 618 (2016).
20. A. S. Aleksandrovsky, A. M. Vyunyshev, A. I. Zaitsev, *et al.*, Quantum Electron. **41**, 748 (2011).
21. V. Petrov, F. Noack, D. Shen, *et al.*, Opt. Lett. **29**, 373 (2004).
22. H. R. Philipp and E. A. Taft, J. Phys. Chem. Solids **1**, 159 (1956).
23. J. Thielking, K. Zhang, J. Tiedau, *et al.*, New J. Phys. **25**, 083026 (2023).
24. A. S. Aleksandrovsky, A. M. Vyunishev, I. E. Shakhura, *et al.*, Phys. Rev. A **78**, 031802 (2008).
25. M. Scholz, D. Opalevs, P. Leisching, *et al.*, Opt. Express **20**, 18659 (2012).
26. A. D. Ludlow, M. M. Boyd, J. Ye, *et al.*, Rev. Mod. Phys. **87**, 637 (2015).
27. D. Perlov, A. Zaytsev, A. Zamkov, *et al.*, "Method for manufacturing of patterned SrB_4BO_7 and PbB_4O_7 crystals," U.S.patent11,868,022 (2024).